FACTA UNIVERSITATIS
Series: **Mechanics, Automatic Control and Robotics** Vol. 6, N° 1, 2007, pp. 119 - 130

CRITICALLY SHAPED CHARGE JET STRESS CAUSED BY ANGULAR VELOCITY

UDC 531.3/539.56:539.42(045)=111

Marinko Ugrčić, Stevan Maksimović

Military Technical Institute, Ratka Resanovića 1, 11132, Belgrade, Serbia

Abstract. *The angular velocity of the shaped charge jet around axial symmetry axis during activation of the shaped charge warhead, especially in the gyroscopic stabilised projectiles, causes intensive changes of the internal stress and deformation state in the jet material. The radial rupture of the shaped charge jet appears under high values of the angular velocity that has the negative consequences on the effectiveness of the warhead, because the drastic penetration reducing. In this way, the qualitative and quantitative determination of the stress and deformation state in the jet material was carried out by finite elements method. The computation of the critical stress in some segments of the shaped charge jet under low angular velocities of the projectile was performed for both cases the elastic and elastic-plastic behaviour of jet material. The nonlinear analysis was attended primary to determine the critical values of angular velocities when maximum stress in jet material equals to the fracture tensile strength.*

Key words: *shaped charge warhead, shaped charge jet, determination of the stress and deformation, finite elements method*

1. INTRODUCTION

The shaped charge is a special explosive device (Fig. 1a) that has been used for both military and civilian industry for different purposes, for example: penetrating, cutting, shaping, welding, etc. Today, most applications of this technology are founding in the oil and gas industry where shaped charges have been used to open up the rocks around drilled wells. The process of the shaped charge jet forming (Fig. 1b) as well as the jet penetration into homogenous obstacle (Fig. 1c), generally, like other similar phenomena in the field of physics of explosion, belong to the class of the problems of nonlinear mechanics, and it can be described very successfully by the equations of the fluid mechanics and high strain phenomena including the shock wave theory. It is possible because of the enormously high values of the velocities, pressures and temperatures that follow this process when the liner and obstacle materials behaviour is similar to the fluid behaviour.

Received March 28, 2007

During the detonation of explosive, the detonation front advances through the explosive creating a temporary very high pressure in the reaction zone. Jet formation by shaped charge has four principal stages: (i) acceleration of the liner by the explosive, (ii) inertial collapse toward the axis of symmetry, (iii) jet and slug formation at the collision junction, (iv) jet elongation until either a target is hit or jet particulates.

When the detonation wave, generated by an explosion, reaches the conical metal liner, the intense pressure forces the tip of the cone to collapse when the jet start to emerge at a high velocity. The main effort consisted in obtaining the longest, non-fragmented, high density jets in order to get a high kinetic energy at the impact.

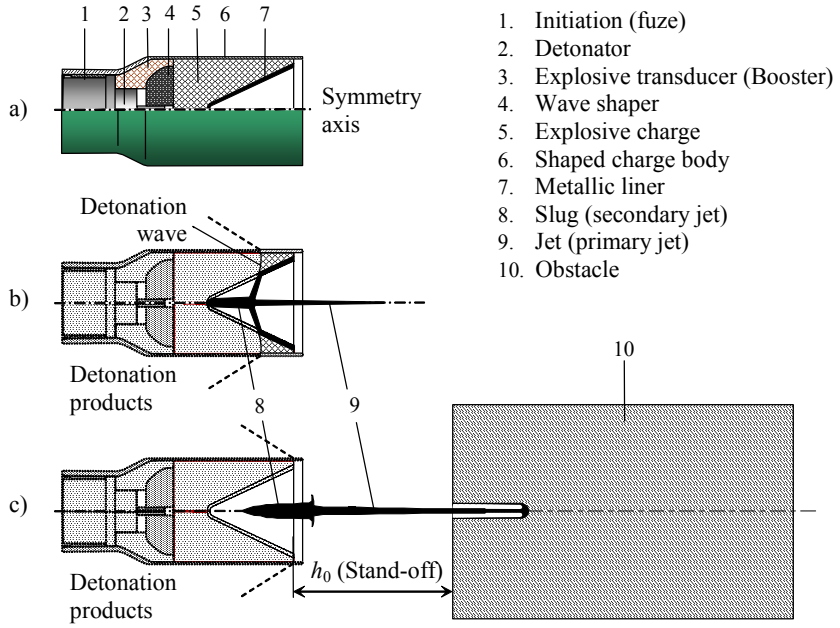

Fig. 1. Schematic review of the shaped charge effect: a) Shaped charge; b) Metallic liner collapsing and shaped charge jet forming; c) Shaped charge jet penetration into obstacle

Whereas the early work was based on trial-and-error experiments, since the 1970s, hydrocodes have been used with some success to predict how a shaped charge would behave. Excellent summaries of shaped charge applications and analytical models are given by Zukas [1], Meyers [2], and in one of the best monograph in the world [3].

The numerical simulation of the shaped charge effect, well-known as cumulative effect, besides the modern software based on the finite elements and/or finite differences codes, can be successfully resolved using the analytical programs based on hydrodynamic theory. The program code HYDRO [4,5] for the numerical simulation of the shaped charge function and jet penetration, make it possible to calculate more accurately the jet kinematical parameters and its penetrability in the obstacles of different mechanical properties.

Analytical models that describe formation of the jet, its elongation and the penetration of target play an important role in the optimization of shaped charges. A number of such models were developed over the world during last years [6,7]. The results of Russian

development of such an analytical methodology and an example of its application for a shaped charge optimization are presented in reference [8].

Several attempts have been made during the last years to model shaped charge jet break-up phenomenon. It is quite clear that the process which the jet goes through during its elongation is very complicated. In addition to the macroscopic mechanical process described by Chou and Carleone [9] the elongation of 1000% and more brings the material microscopically to an exceptionally anisotropic state [10].

Finite elements method (FEM) can be used for more qualitative numerical simulations of the formation, fragmentation, and penetration in a plate of a copper jet that develops in a shaped charge. Camacho [11] was described the computational methodology in greater details. In this paper, the focus is on jet breakage.

But extremely complicated phenomenon represents the radial rupture of the shaped charge jet that appears under high values of the angular velocity. Its spin rate has very negative consequences on the effectiveness of the shaped charge, because of the drastic reducing of jet penetration. In this way, the qualitative and quantitative determination of the stress and deformations state in the jet material is very important input parameter to design and optimise the shaped charge.

2. THEORY

The analytical program code was used to define necessary geometrical and kinematical parameters during forming phase and after, during post-forming phase, i.e. rotating jet evolution until a target is hit. The final analysis included finite elements method (FEM) used to determine the stresses and deformations of shaped jet caused by itself rotation about proper symmetry axis. In this way some approximations concerning the form as well as the axial and angular velocity of the jet were involved in the analysis.

2.1. Shaped charge jet evolution (jet equations)

The numerical determination of the geometrical and kinematical parameters of the jet (jet equations), schematically shown in Fig. 2, was developed based on the hydrodynamic theory and utilizes the established laws of conservation of mass, energy, and momentum.

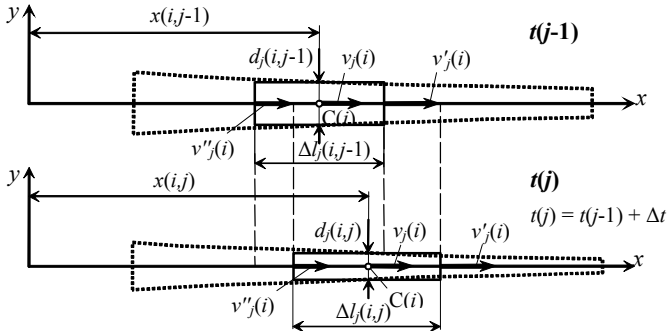

Fig. 2. The changes of the placement, length and radius of the jet during evolution

With known initial values of the length $\Delta l_{j0}(i)$ and diameter $d_{j0}(i)$ of the jet element i at the moment of forming t_f, as well as the velocities of the frontal $v'_j(i)$ and rear $v''_j(i)$ side of the jet element cross-section, it is possible to calculate each parameter of jet evolution. So, the changes of the placement $x_j(i,j)$ of the centre of jet element mass C(i), length $\Delta l_j(i,j)$ and radius $r_j(i,j)$ of the jet element i during evolution at he moment $t(j)$ are given by equations

$$x(i,j) = x_{i0} + v_j(i)\ t(j) \tag{1}$$

$$v'_j(i) = \frac{v_j(i) + v_j(i\text{-}1)}{2} \tag{2}$$

$$v''_j(i) = \frac{v_j(i) + v_j(i\text{+}1)}{2} \tag{3}$$

$$\Delta l_j(i,j) = \Delta l_{j0}(i) + [v'_j(i) - v''_j(i)]\ t(j) \tag{4}$$

$$r_j(i,j) = \frac{1}{2}\sqrt{\frac{\Delta V_j(i)}{\pi\ \Delta l_j(i,j)}} \tag{5}$$

where is:

$\Delta V_j(i)$ – volume of the jet element.

The values of the angular velocity of jet elements were calculated based on the law of conservation of momentum. The equation is given in the integral form

$$\omega_j(i) = \omega_0 \left(\frac{r(i)}{r_j(i)} \right)^k \tag{6}$$

where is:

$\omega_j(i)$ – jet element angular velocity [or jet spin rate $n_j(i)= 60\omega_j(i)/2\pi$ in rev/min],
ω_0 – angular velocity of the shaped charge,
$r(i)$ – radius of the liner element (cross-section i),
$r_j(i)$ – radius of the jet element at the moment of colliding with obstacle, and
k – empirical coefficient.

In accordance to the law of conservation of momentum $k = 2$, but it takes significantly lower values caused by very intensive inter-crystal friction in material of the jet as well as the friction between the external side of collapsing metallic cone and products of detonation.

The model of 60 mm shaped charge (Fig. 3) was used for theoretical analysis and experimental testing considered in this paper.

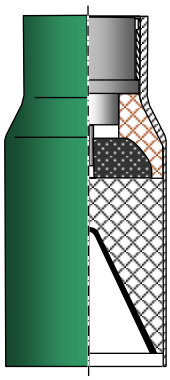

Main geometrical and physical characteristics of the experimental shaped charge model

- Calibre: 60 mm
- Explosive charge: flegmatized octogen (average density 1.75 g/cm^3)
- Booster: flegmatized hexogen (average density 1.71 g/cm^3)
- Detonator: pentryte (average density 1.61 g/cm^3)
- Metallic body: duralumin (density 2.75 g/cm^3)
- Thickness of metallic body: 1.5 mm
- Wave-shaper: inert plastic mass
- Initiation: punctually by electrical igniter
- Angle of copper liner cone: 50°

Fig. 3. Axial cross-section of the experimental model of 60 mm shaped charge

Calculated values of the geometrical and kinematical parameters of the jet of 60 mm shaped charge at the moment of colliding with obstacle (stand-off h_0 = 200 mm) are given in the Table 1.

Table 1. Calculated geometrical and kinematical parameters of 60 mm shaped charge jet

Segment	Liner element radius	Jet element velocity	Jet element length	Jet element radius	Jet element rotation rate
i	$r_j(i)$	$v_j(i)$	$\Delta l_j(i)$	$r_j(i)$	$n_j(i)$
(-)	(m)	(m/s)	(m)	(m)	(rev/min)
1	0.00215	8846.862	0.00412	0.00139	2392
2	0.00310	8770.069	0.00423	0.00159	3801
3	0.00447	8646.862	0.00673	0.00196	5201
4	0.00499	8425.893	0.00914	0.00211	5593
5	0.00594	8285.999	0.01054	0.00221	7224
6	0.00689	7815.563	0.01376	0.00213	10463
7	0.00784	7348.542	0.01348	0.00216	13174
8	0.00878	6873.141	0.01344	0.00222	15642
9	0.00973	6377.237	0.01371	0.00231	17742
10	0.01068	5847.988	0.01421	0.00242	19476
11	0.01162	5270.793	0.01500	0.00257	20443
12	0.01257	4628.065	0.01597	0.00276	20742
13	0.01352	3897.341	0.01715	0.00297	20722
14	0.01446	3048.532	0.01823	0.00315	21072
15	0.01533	2315.969	0.01511	0.00392	15293

2.2. The stress analysis of shaped charge jet by finite elements

As it is above mentioned, the main effort consisted of obtaining the longest, non-fragmented, and high-density jet in order to get a high kinetic energy at impact. To obtain the

jet of given characteristics, the computation of the stress and deformation in some segments of the shaped charge jet during its forming and evolution until colliding with the obstacle is very important. The attention in this paper was focused on the stress and deformation analysis of jet caused by the angular velocities only.

The computation of the stress and deformations in some segments of shaped charge jet, with different values of the angular velocities of jet, was considered and carried out by the use of finite elements method (FEM) [12]. The FEM there was of special interest to determine the critical stresses of jet. For this purpose the conical part of jet under the angular velocities ω, was treated. The main geometry and material properties of the conical part of shaped charge jet modelled for the FEM analysis are shown in Fig. 4 and Table 2 [13], respectively.

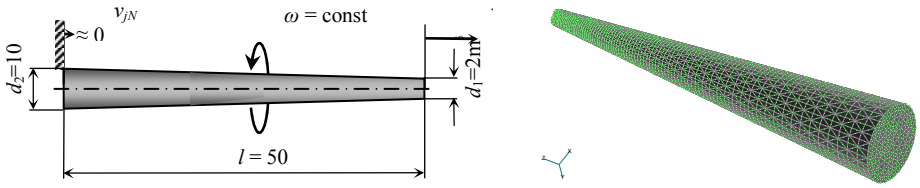

Fig. 4. Mathematical model of the part of rotating jet prepared for the FEM analysis

Table 2. Material properties of the metallic liner (Copper C2200)

Parameter	Denotation	Dimension	Value
Mass density	ρ	kg/m^3	8800
Young's modulus	E	GPa	115
Poisson's ratio	v	-	0.307
Initial yield stress	σ_y	MPa	206.8
Reference plastic strain	ε_0^p	-	0.08
Reference plastic strain rate	$\dot{\varepsilon}_0^p$	s^{-1}	0.1
Rate sensitivity exponent 1	m_1	-	20
Rate sensitivity exponent 2	m_2	-	10
Hardening exponent	n	-	4.8
Threshold strain rate	$\dot{\varepsilon}_t$	s^{-1}	5000
Fracture tensile strength	σ_{ten}	MPa	310
Heat capacity	c	J/kgK	376
Heat conductivity	k	W/mK	189
Referential temperature	T_{ref}	K	293.3
Melting temperature	T_{melt}	K	1318.3
Softening exponent	α	-	1.0
Friction coefficient	μ	-	0.01
Taylor-Quinney Beta	β	-	0.9

The typical redesigned curve that represents stress strain dependence versus relative deformation of the metallic liner (Copper C2200) is shown in Fig. 5.

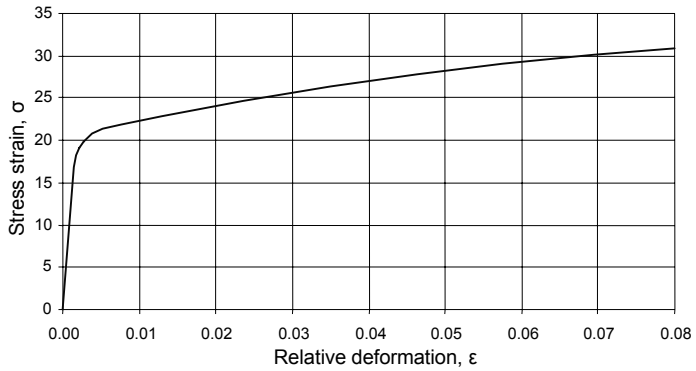

Fig. 5. Elastic-plastic stress strain material behaviour of Copper C2200

In order to prepare the mathematical model (Fig. 4) of the shaped charge jet and adapt it for easier FEM analysis, as the first approximation carried out in this paper, we assumed as follows:

– the initial form of the jet is an ideal cone,
– the rotation along the length of jet is uniform and equals (ω = const.),
– the end part of the jet is clamped, i.e. it has not possibility to move axially ($v_{jN} = 0$),
– the top of the jet moves with maximum jet velocity v_{j0}, and
– the fracture tensile strength R (or σ_{ten}) is actual for static conditions. The relevant, real dynamical values of the fracture tensile strength is significantly greater then this one.

3. NUMERICAL ANALYSIS AND DISCUSSION OF RESULTS

Main computation results given by the FEM are shown in Figs. 6 to 15. The primary attention of these analyses was to determine the critical values of angular velocities ω_{cr}, i.e. n_{cr}, when maximum stress in jet material equals to the fracture tensile strength σ_{ten}.

3.1. Elastic stress analysis by finite elements

The critical value n_{cr} that correspond to maximum value of von Misses stress (fracture tensile strength of copper) is determined fixing the end surface of jet by two different manners.

The results of the numerical analysis of first type of jet end surface fixing are illustrated in Figures 6 and 7. These figures illustrate the pre-processed finite elements mesh with nodal fixed points at the end surface of the jet and the stress distributions of the conical shaped charge jet for maximum allowed value of the angular velocities of projectile, respectively. As well, it is shown that the critical values of spin rate of the jet is n_{cr}=5880 rev/min.

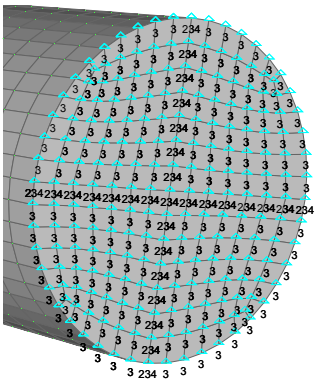

Fig. 6. Finite elements grid with nodal fixed points

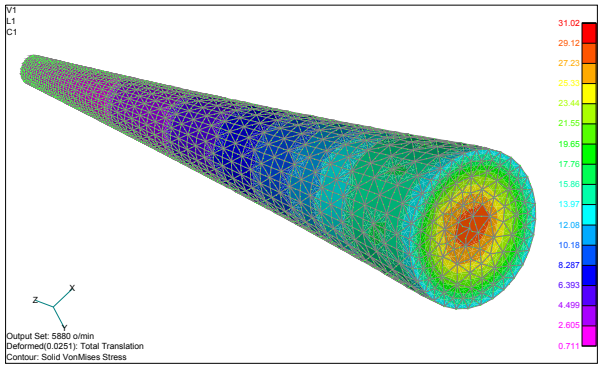

Fig. 7. Stress distributions of the jet for fully fixed end surface (n_{cr}=5880 rev/min)

Analogically, the results of the second type of fixing of the end surface of jet are illustrated in Figures 8 and 9. These figures illustrate the pre-processed finite elements mesh with partially nodal fixed points at the end surface of the jet as well as the stress distributions of the conical shaped charge jet for same value of the angular velocities of projectile. In this case, partially fixed end surface of the jet causes the initialisation of forming of the round rear part of jet.

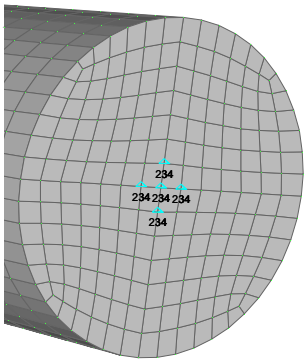

Fig. 8. Finite elements grid with nodal fixed points

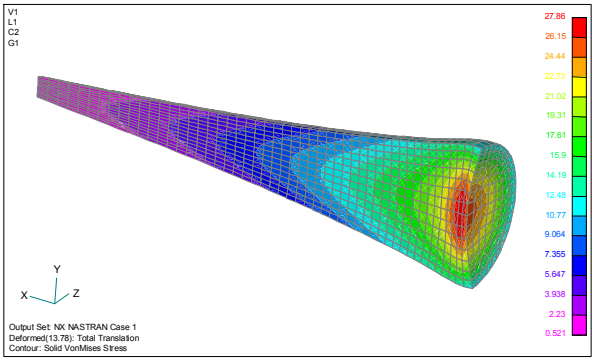

Fig. 9. Stress distributions of the jet for partially fixed end surface (n=5880 rev/min)

The analysis of the FEM calculation (Fig. 6 to 9) shows that critical stress zone appears evidently in the rear part of the jet where its thickness is the greatest.

3.2. Elastic-plastic stress analysis by finite elements

As well, the identical procedure was carried out by elastic-plastic stress analysis by finite elements method. The results are shown in Fig. 10 and 11.

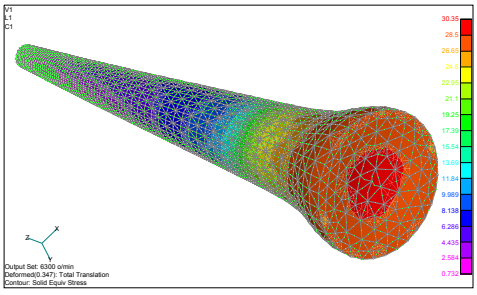

Fig. 10. Stress distributions of the jet (n=6300 rev/min)

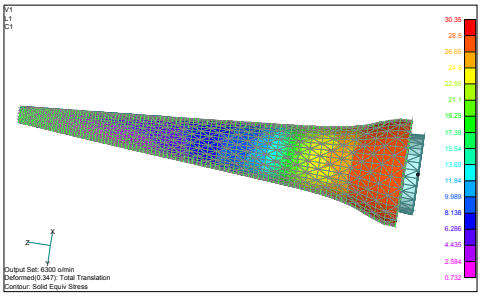

Fig. 11. Stress distributions and displacements of the jet (n=6300 rev/min)

Figures 10 and 11 show that critical stress zone appears in the rear part of the jet at spin rate of n=6300 rev/min. As well, the rotation causes very intensive contraction of cross-sections in the frontal zone of the jet and itself radial spreading in rear part. At same time, the total length of the jet shortens for more then 5 percents.

In order to compare the results of numerical analysis the stress distributions over the cross section and stress distributions and displacements over the axial cross section of the jet for both the FEM analysis the elastic and elastic-plastic are shown in Figures 12 to 15.

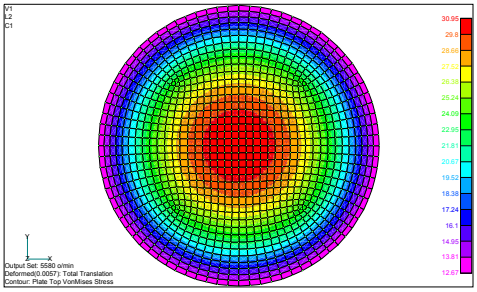

Fig. 12. Stress distributions at the end surface of jet given by the elastic FEM (n=5880 rev/min)

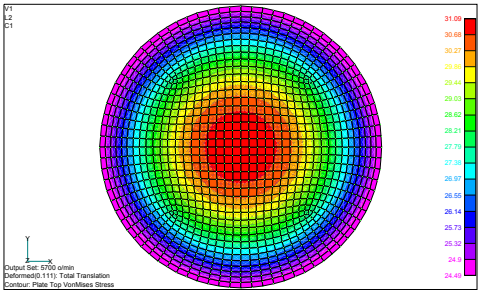

Fig. 13. Stress distributions at the end surface of jet given by the elastic-plastic FEM (n=6300 rev/min)

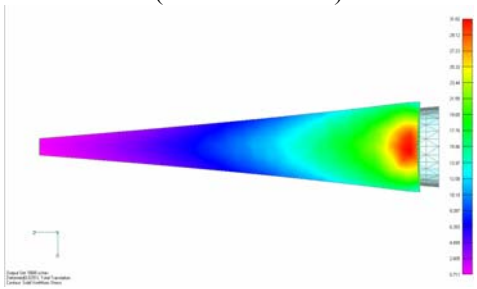

Fig. 14. Stress distributions of the jet given by elastic FEM (n=5880 rev/min)

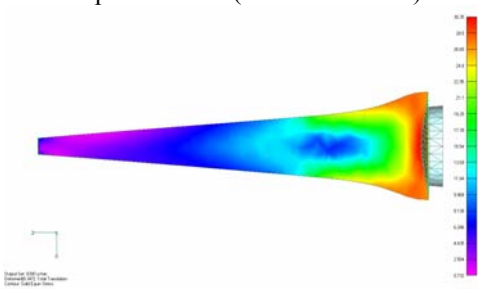

Fig. 15. Stress distributions of the jet given by elastic-plastic FEM (n=6300 rev/min)

The comparative analysis of the numerical results given by the elastic and elastic-plastic FEM shows that the critical stress strains appear earlier in the case of pure elastic behaviour of jet material, i.e. at the spin rate n=5880 rev/min, that is smaller for 6 percents in comparison with the case of the elastic-plastic behaviour of same material (n=6300 rev/min). As well, the plastic phase in the behaviour of the material produces same differences between the stress and displacements of jet material (Fig. 14 and 15).

4. EXPERIMENTAL TESTING AND DISCUSSION OF RESULTS

In order to verify the theoretical prediction some experimental testing was carried out. The experimental testing was included range testing of the penetrability of rotating shaped charge as well as the laboratory testing by use of the techniques of impulse radiography [14-16].

The penetrability testing was carried out at the terminal ballistics laboratory using mobile rotating device with special equipment (Fig. 16) described in [17]. Besides the remote control of shaped charge activation it gave possibilities to testing shaped charge jet penetrability depending on charge spin rate from 800 to 6000 rev/min.

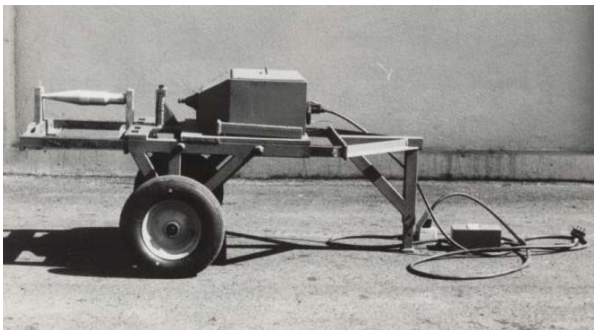

Fig. 16. Special device with equipment for penetrability testing of rotating shaped charges

Figure 17 shows the radiographs of the 60 mm shaped charge jet at moment of total liner collapsing and complete jet forming (10 a) and at the moment of the collision between the jet and the obstacle (10 b), respectively.

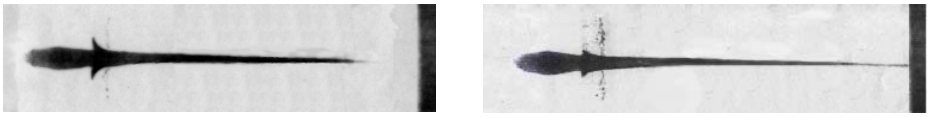

a) b)

Fig. 17. Radiographs of 60 mm shaped charge jet ($\omega_0 = 0$):
a) at the moment of total liner collapsing; b) collision of the jet and obstacle

The comparative analysis of the numerical data of geometrical parameters of the jet given in the Table 1 and radiograph in Fig. 17 are in a good accordance.

Also, the technique of impulse radiography was used to clarify the process of the jet and slug separation (Fig. 18).

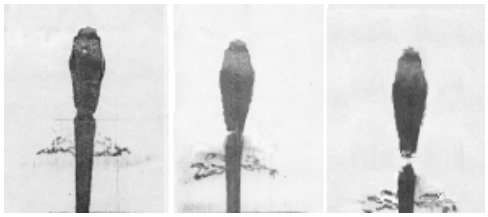

Fig. 18. Radiographs of jet and slug separation (rounding of the rear part of the jet)

Radiographs in Fig. 18 shows that the adhesive forces between the jet and slag causes rounding of the rear part of the jet. This fact justifies the earlier assumed prediction meaning that the jet is partially clamped over its end surface (Fig. 9).

The penetrability was tested with two specimens containing 10 shaped charges at zero rotation (n_0=0 rev/min) and rotation of n_{1000}=1000 rev/min. Relevant jet output piercing holes at the end side of obstacle are shown in Figure 19.

a) n_0 = 0 rev/min b) n_{1000} = 1000 rev/min

Fig. 19. Output piercing holes of the jet at the end side of 40 mm thick obstacle

Based on the analysis of pictures in the Figure 19 can be concluded that the increasing of the spin rate of shaped charge produces the increasing of piercing hole diameter and at same time causes decreasing of the jet penetrability. These statements are in very good accordance with the FEM numerical results given in Figures 14 and 15.

5. CONCLUSIONS

The analysis of the specific dependences of the shaped charge jet feature as well as the stress and deformation in the jet under the low value of its angular velocity was clarified. The finite element method was successfully used to define the critical spin rate of shaped charge when jet material gets the fracture tensile strength.

In order to determine the stress distributions and displacements over the axial cross section of the jet, two types of the FEM analysis - the elastic and elastic-plastic behaviour of jet material were carried out. The comparative analysis of given computation results shows that the critical stress strains appear earlier in the case of pure elastic behaviour of jet material that is smaller for 6 percents then in the case of elastic-plastic behaviour of same material. At same time, the plastic phase of jet material behaviour produces same differences between the stress and displacements of jet structure.

As well, it is shown that the critical stress zone appears in the rear part of the jet where its diameter becomes the greatest. The rotation causes very intensive contraction of cross-sections in the frontal zone of the jet and itself radial spreading in the rear part. At same time, the total length of the jet shortens significantly and causes an evident decreasing of the jet penetrability.

The laboratory testing of the experimental shaped charge, confirming the discussed theoretical predictions given by use the hydrodynamics theory and the FEM calculations, has shown very good overlapping of the theoretical and experimental results.

Acknowledgement: *Parts of this research were supported by the Ministry of Science and Environment Protection of Republic Serbia trough Mathematical Institute SANU Belgrade Grant ON144002*

"Theoretical and Applied Mechanics of Rigid and Solid Body, Mechanics of Materials" and Ministry of Defence of Republic Serbia – Military Technical Institute.

REFERENCES

1. Zukas, J.A., (1990), High Velocity Impact Dynamics, *Wiley*, New York, USA
2. Meyers, M.A., (1994), Dynamic Behaviour of Materials, *Wiley*, New York, USA
3. Baum, F.A., Stanjukovich, K.P., Schehter, B.I. (1975), Fizika vzriva, Second and adapted edition, Moscow
4. Ugrčić, M., (1998), Numerical Simulation and Optimisation of the Shaped Charge Function*, Scientific Technical Review*, Vol. XLVIII, Num. 4, pp. 30-41, (in Serbian)
5. Ugrčić, M., (2003), Determination of the Critical Jet Velocity During the Penetration into the Homogenous Steel Obstacle, *Series Mechanics, Automatic control, and Robotics, Facta universitatis*, Vol. 3. No15, Niš, pp. 981-988.
6. Chou, P.C and Carleone, J., (1977), The stability of Shaped Charge Jet Break-up Time, *J. Appl. Phys.*, 48, pp. 4187-4195.
7. Hirsch, E., A, (1981), Model for Explaining the Rule for Calculating the Break-up Time of Homogeneous Ductile Metals, *Propellants Explosives & Pyrotechnics*, 11. pp.
8. Arlow, A.J, Curtis J.P., (1995), Analytic Computer Models for the Design and Evaluation of Shaped Charges, *Proc. The 15th Int. Symp. Ballistics*, Vol 2, Jerusalem, Israel, pp. WM/211-218.
9. Sofronov, I.D, Ilkaev, R.I, Kovalev, N.P, Svirsky, O.V., (1997), Calculation of sharped charge performance, *Proc. Int. Seminar on Fundamental Problems of Cumulation*, St. Petersburg, Russia, pp. 230-259.
10. Swirsky, O.V., Vlasova, M.A., Korotkov, MI, Krutyakov, VA, Toropova, TA., (2003), The Analytical Model ATOS-M for Computing of the Shaped Charge Jet Penetration Parameters, *Int. J. Impact Engineering, 29*, pp. 683-690.
11. Camacho, G.T., Ortiz, M., (1997), Adaptive Lagrangian Modelling of Ballistic Penetration of Metallic Targets, *Comput. Methods Appl. Mech. Eng*., 142, pp. 269–301.
12. MSC/NASTRAN Theoretical Manuals
13. ASM International, (Ed.), Metals Handbook, Vol. 2, Properties and Selection: Nonferrous Alloys and Special-Purpose Materials, 1990.
14. Ugrčić, M., (1989), Contribution to the General Method of the Experimental Researching of the Shaped Charge Effect with Special Attention On The Experimental Researching of the Rotation Influence on the Shaped Charge Penetrability, *Scientific Technical Review*, Vol. XXXIX, Num. 7, pp. 27-34, (in Serbian)
15. Ugrčić, M., (1988), Rotation Influence on the Shaped Charge Effect, *Book E, 17th Symposium on explosive materials JKEM*, Lučani, pp. 81-95, (in Serbian)
16. Ugrčić, M., (2002), The Study of the Use Possibility of the Semi-Destructive Method for the Shaped Charge Quality Testing", *20th International Symposium on Ballistics*, Orlando, Florida-USA, pp. 635-643.
17. Ugrčić, M.., (1985), Equipment for Static Testing of the Rotation Influence on the Shaped Charge Effect, *Technical Report*, VTI-02-23-329, Belgrade, (in Serbian)

KRITIČNI NAPON U KUMULATIVNOM MLAZU IZAZVAN ROTACIJOM

Marinko Ugrčić, Stevan Maksimović

Obrtanje kumulativnog mlaza oko uzdužne ose pri dejstvu kumulativne bojne glave, posebno kod žiroskopski stabilisanih projektila, izaziva intenzivne promene unutrašnjeg naponsko-deformacionog stanja u materijalu mlaza. Pri visokim nivoima ugaone brzine dolazi do pojave radijalnog kidanja kumulativnog mlaza što ima negativne posledice na efikasnost bojne glave, jer dovodi do drastičnog pada probojnosti. Kvalitativno i kvantitativno određivanje naponsko-deformacionog stanja u materijalu mlaza izvršeno je metodom konačnih elemenata. Proračun napona i deformacija u određenim segmentima kumulativnog mlaza, pri malim vrednostima rotacije projektila, urađen je za dva slučaja, elastični i elasto-plastični model mlaza.

Ključne reči: *Kumulativna bojna glava, kumulativni mlaz, određivanje napona i deformacija, metoda konačnih elemenata*